Atmos. Chem. Phys. Discuss., 12, 10845–10878, 2012
www.atmos-chem-phys-discuss.net/12/10845/2012/
doi:10.5194/acpd-12-10845-2012

Atmospheric Chemistry and Physics Discussions

Seasonal and diurnal variations of atmospheric mercury across the US determined from AMNet monitoring data

X. Lan[1], R. Talbot[1], M. Castro[2], K. Perry[3], and W. Luke[4]

[1]Institute for Multidimensional Air Quality Studies, Department of Earth & Atmospheric Sciences, University of Houston, Houston TX 77004, USA
[2]Center for Environmental Science, University of Maryland, Frostburg, MD 21532, USA
[3]University of Utah, Salt Lake City, UT 84112-0110, USA
[4]National Oceanographic and Atmospheric Administration, Air Resources Laboratory, Silver Spring, Maryland 20910, USA

Received: 27 March 2012 – Accepted: 11 April 2012 – Published: 26 April 2012

Correspondence to: X. Lan (xlan3@uh.edu)

Published by Copernicus Publications on behalf of the European Geosciences Union.

Abstract

Speciated atmospheric mercury observations collected over the period from 2008 to 2010 at the Environmental Protection Agency and National Atmospheric Deposition Program Atmospheric Mercury Network sites (AMNet) were analyzed for its spatial, seasonal, and diurnal characteristics across the US Median values of gaseous elemental mercury (GEM), gaseous oxidized mercury (GOM) and particulate bound mercury (PBM) at 11 different AMNet sites ranged from 148–226 ppqv (1.32–2.02 ng m^{-3}), 0.05–1.4 ppqv (0.47–12.4 pg m^{-3}) and 0.18–1.5 ppqv (1.61–13.7 pg m^{-3}), respectively. Common characteristics of these sites were the similar median levels of GEM as well as its seasonality, with the highest mixing ratios occurring in winter and spring and the lowest in fall. However, discernible differences in monthly average GEM were as large as 30 ppqv, which may be caused by sporadic influence from local emission sources. The largest diurnal variation amplitude of GEM occurred in the summer. Seven rural sites displayed similar GEM summer diurnal patterns, in that the lowest levels appeared in the early morning, and then the GEM mixing ratio increased after sunrise and reached its maxima at noon or in the early afternoon. However, sites in Utah (UT96, UT97) and New York (NY95) showed a distinctly different pattern, with the lowest mixing ratios appearing in the afternoon and the highest mixing ratios at night. Unlike GEM, GOM exhibited higher mixing ratios in spring and summer. The largest diurnal variation amplitude of GOM occurred in spring for most AMNet sites. GOM diurnal minima appeared before sunrise and maxima appeared in the afternoon, and the variation in magnitude for all seasons at most monitoring sites fell in the range of 0 to 2 ppqv, except the Utah sites (up to 5 ppqv). The increased GOM mixing ratio in the afternoon indicated a photochemically driven oxidation of GEM resulting in GOM formation. PBM exhibited diurnal fluctuations in summertime instead of wintertime, although the PBM mixing ratio in summer was not as high as in winter. The summertime PBM diurnal pattern displayed a daily maximum in the early afternoon and lower mixing ratios at night, implying photochemical production of PBM in summer. The marine sea salt aerosol

ACPD

12, 10845–10878, 2012

uptake of GEM and GOM was not apparent in the PBM data collected at coastal sites, with PBM being higher at inland sites.

1 Introduction

Mercury is an important environmental pollutant that can enter the food chain and pose threats to ecosystems and human health (EPA, 1997). Atmospheric mercury exists in three different chemical forms that consist of gaseous elemental mercury (GEM = Hg^0), gaseous oxidized mercury (GOM = $HgCl_2$ + $HgBr_2$ + HgOBr + . . .) and particular bound mercury (PBM). GEM is reported to be the predominant (~95 %) atmospheric mercury species (Lindberg and Stratton, 1998), with a relatively long lifetime (6–24 months) that enables its global transport (Weiss-Penzias et al., 2003). GEM can be oxidized to GOM by ozone (O_3), hydroxyl radical (OH), nitrate radical (NO_3), and halogen radicals (Pal and Ariya, 2004a, b; Sommar et al.,2001; Calvert and Lindberg, 2005; Sommar et al., 1997; Laurier et al., 2003; Raofie and Ariya, 2004; Holmes et al., 2006, 2010), part of which can be converted to PBM on aerosol surfaces. GOM and PBM account for a small fraction of atmospheric mercury and are thought to be readily deposited on the order of 1–7 days near emission sources (Valente et al., 2007). The sources of atmospheric mercury consists of various anthropogenic emissions (e.g., coal combustion, waste incineration and transportation) (Seigneur et al., 2004, 2006) and natural sources (e.g., mercury enriched soils, the ocean and volcanoes) (Pacyna et al., 2002, 2006, 2010; Sigler et al., 2003; Sigler and Lee, 2006; Brunk et al., 2001; Friedli et al., 2011, 2003a, b, 2004; Ebinghaus et al., 2007), resulting in great diversity in mercury levels around the world.

A recent review by Sprovieri et al. (2010) reported that the current global background concentration of GEM was in the range of 1.5 to 1.7 ng m^{-3} (168–190 ppqv) in the Northern Hemisphere. Continuous monitoring datasets at two coastal sites in Europe (Mace Head and Zingst) showed that the annually total gaseous mercury (TGM = GEM + GOM) concentrations were 1.72 ng m^{-3} (193 ppqv) at Mace Head and 1.66 ng m^{-3}

ACPD
12, 10845–10878, 2012

(186 ppqv) at Zingst (Kock et al., 2005). Long-term measurements at the Canadian Atmospheric Mercury Measurement Network (CAMNet) reported that the 10 yr averaged TGM concentrations of all CAMNet sites was 1.58 ng m^{-3}, lower than European records (Temme et al., 2007). A study in Reno, a city in the western US apparently influenced by regional mining, showed a 3-yr average GEM value of 1.6 ng m^{-3} (179 ppqv) and an exceptionally high GOM value of 26 pg m^{-3} (2.9 ppqv). Distinct seasonality was found, with the highest GEM concentrations in winter and highest GOM concentrations in summer (Peterson et al., 2009). For rural and mountainous sites in northeastern and southeastern US, Sigler and Lee (2006) and Valente et al. (2007) suggested typical levels of GEM were about 1.6 ng m^{-3} (179 ppqv).

The Atmospheric Mercury Network (AMNet) is a long-term monitoring network in the United States aimed at quantifying the ambient levels of speciated mercury across the US. A few published analyses on these sites documented regional mercury levels, mercury sources and its temporal variation. Measurements in a rural area in the Northeast, the Adirondacks of New York State (NY20), showed that the average concentrations of GEM, GOM and PBM were 1.4 ± 0.4 ng m^{-3}, 1.8 ± 2.2 pg m^{-3}, and 3.2 ± 3.7 pg m^{-3}, respectively (Choi et al., 2008); whereas the Rochester (NY95) urban site exhibited GEM, GOM and PBM concentrations of 1.49–1.52 ng m^{-3}, 1.83–8.70 pg m^{-3}, 4.70–7.48 pg m^{-3}, slightly higher than at the Huntington Wildlife (NY20) site. Melting snow, chemical oxidation, coal fired power plant and mobile emissions during rush hours were identified as important factors influencing speciated mercury variations in Rochester (Huang et al., 2010). Temporal variability of ambient mercury levels reflect the effects of chemical and physical sources and sinks, which are of great importance in understanding the regional mercury budget. Analysis of data obtained at Thompson Farm, a rural AMNet site in New Hampshire (NH06), found noticeable GEM daily patterns in summer and fall with the daily maximum occurring around 10:00 and minimum at 05:00–06:00 Eastern Standard Time (EST). GOM peaked at midday with seasonal daily maxima ranging from 0.5 ppqv (summer/fall) to 1.6 ppqv (spring) (Sigler et al., 2009). GOM levels at Appledore Island (a marine site near NH06) were higher than

ACPD
12, 10845–10878, 2012

at NH06 suggesting the possibility that GEM was oxidized by abundant halogen radicals in the marine environment leading to higher GOM mixing ratios (Mao and Talbot, 2011). Measurements at a rural site in the Ohio River Valley region (OH02) showed that the GEM diurnal pattern had the highest levels at midday. GOM mixing ratios reached maximum values at noon and then slowly decreased throughout the rest of the day to a minimum at 06:00. Because the GOM maxima coincided with afternoon elevated ozone and temperature, GOM diurnal variation in Ohio may be associated with regional transport of photochemically processed air masses (Yatavelli et al., 2006).

To date there has not been an in-depth analysis across all AMNet sites to document continental scale mixing ratios of mercury, and their seasonal and diurnal variability. A large-scale picture of speciated mercury in the US is needed for an improved detailed understanding of the distribution on various temporal and spatial scales, and to better inform regional and global models.

2 Measurements and approach

2.1 AMNet sites

The Atmospheric Mercury Network (AMNet) is one of the monitoring networks in the Environmental Protecton Agency and National Atmospheric Deposition Program in the US, designed to provide information on mercury in precipitation, deposition chemistry, and its phase fractionations in ambient air. This network includes more than 20 automated speciated mercury sampling sites, including some cooperating sites outside the U.S. Continuous measurement data from 2008 to 2010 were recorded at 11 sampling sites, which were examined in detail in this study to demonstrate the seasonal and diurnal oscillations of mercury levels. These sites included Mississippi (MS12), Oklahoma (OK99), Utah (UT96 and UT97), Ohio (OH02), Maryland (MD08), New York (NY95, NY20), New Hampshire (NH06), Vermont (VT99) and Nova Scotia (NS01)(Fig. 1). Except NY95 and UT97, all the sampling sites were rural sites with no significant

ACPD
12, 10845–10878, 2012

emission sources within their 10 km radius. Detailed sites descriptions and local emission strengths calculated from 2005 National Emission Inventory are list in Table 1.

2.2 Measurements and data

Speciated mercury was measured in this network by a suite of automated Tekran mercury instrumentation. GEM is measured via a cold vapor atomic florescence (CVAF) spectrometer (Model 2537A or B) in a sequential dual channel mode with 5 min time intervals and a detection limit of ~5–10 ppqv (1 ng m^{-3} = 112 ppqv). GOM was measured with a speciation unit (Model 1130) consisting of a KCl coated denuder. PBM was trapped on a quartz frit (Model 1135). GOM and PBM were typically averaged over 2 h and then analyzed for 1 h, and thus the dataset had 3 h time resolution. GEM data presented here are also 3 h time resolution, although the original data was typically 5 min time resolution. It is important to note that all instrumentation was operated in an identical manner according to standard operating procedures agreed to by the site operators. More details on instrument and operating procedures are presented on the AMNet website (http://nadp.sws.uiuc.edu/amn/docs.aspx).

The GEM mixing ratios were always above the detection limit. The detection limit of GOM was estimated to be 0.05–0.1 ppqv, based on three times the standard deviation of average blank values determined at NH06 and NY95 sites (Sigler et al., 2009; Huang et al., 2010). The detection limit of PBM was estimated to be 0.1 ppqv (Huang et al., 2010). No special treatment was applied to the GOM and PBM data that may have been less than the detection limit because, in our analysis, median values were utilized instead of mean values for site comparisons. Hourly diurnal profiles were achieved by utilizing the 2 h measurement data (1 data/2 h) to represent the starting and ending time points, as well as the middle time point.

ACPD
12, 10845–10878, 2012

3 General characteristics

3.1 GEM

The median mixing ratio of GEM was relatively uniform (Fig. 2), and varied within the range of 148–226 ppqv (Table 2), which is similar to the current background mixing ratio of GEM in the Northern Hemisphere (Sprovieri et al., 2010). However, the UT97 sites exhibited a high median level (226 ppqv) and large standard deviation (95 ppqv). It also exhibited frequent large spikes in its time series. From the 2005 National Emission Inventory (Table 1), it is clear that UT97 was heavily impacted by nearby anthropogenic emission sources (i.e., smelting activities, petroleum refining and landfills). The unusual characteristics of this site indicated that the frequent GEM pulses most likely originated from local point sources. The emission sources corresponding to UT97 were similar with UT96, but the median GEM level at UT97 was 50 ppqv higher than at UT96. Considering the elevation of this site, UT97 could also capture long-distance transported mercury, which may include mining and/or Asian emissions. The UT96 showed slightly higher median GEM levels than other rural sites, however, with a high standard deviation similar to UT97. This suggested that local emissions or point sources were very likely to be the dominant factors determining GEM mixing ratios in this region.

The Ohio River Valley has a large number of coal-fired power plants; mercury compounds emitted by the facilities within 150 km radius of OH02 site were estimated to be more than 9 tons yr^{-1} according to the 2005 National Emission Inventory (Table 1). However, the median mixing ratio of GEM at the OH02 site was similar to the overall average for all sites. A feature of OH02 was that it demonstrated an exceptional high standard derivation of about 5–6 times that of other rural sites. Although it had fewer large spikes than UT97, OH02 probably intercepted downwind air masses from nearby point sources (such as coal-fired power plants, clay production and organic chemical industry emissions) frequently.

Coastal sites NS01, NH06 and MD08 showed especially low GEM values in late summer to early fall (<100 ppqv). Comparison between the coastal data (from NS01,

ACPD
12, 10845–10878, 2012

NH06, MD08 sites) and inland data (from all inland sites except NY20) during the mid-July to September period showed a statistically significant difference ($p \leq 0.001$) in their median values (median difference = 15 ppqv) with higher mixing ratios inland. This feature may be caused by the influence of halogens converting GEM to GOM or PBM in coastal areas. Previous research has demonstrated that halogen oxidation of GEM may have substantial influence on GEM abundance for coastal airsheds (Laurier et al., 2003). In-depth analysis of the NH06 data also suggested that halogen chemistry is a reason for the significantly lower GEM levels and steeper decreasing trend during the warm season (Mao et al., 2008). However, the coastal site MS12 does not show especially low values during the late summer-early fall period, although the emission sources near MS12 are not typically different from the NS01, NH06 and MD08 sites. This suggests that meteorological factors, especially wind direction and speed that advect mercury from surrounding industries to the MS12 sampling site could be an important factor for its GEM variation.

Although GEM at sites across the US appeared to mimic each other closely in average value and seasonal temporal changes, discernible differences in mixing ratios can be found in monthly median GEM values (Fig. 2). For the same month, the differences among median values were as large as 30 ppqv (exclude the exceptional high UT97 value). This could result from significantly diverse emission sources and removal mechanisms.

3.2 GOM

The GOM mixing ratio is typically higher in urban or industrial areas, whereas it is lower in rural areas because it is influenced primarily by local and regional sources due to its short atmospheric resident time. Valente et al. (2007) summarized previous global measurements and reported that the mean concentrations of GOM in remote or rural areas was 0.003–0.163 ng m^3 (0.34–18.3 ppqv) with mean value of 0.018 ng m^3 (2.0 ppqv), whereas in urban areas or near-point source sites it was 0.0061–0.121 ng m^3 (0.68–13.5 ppqv) with mean value of 0.052 ng m^3 (5.8 ppqv). Our

ACPD
12, 10845–10878, 2012

analysis of the AMNet dataset, including both rural and urban sites, showed that median GOM values ranged from 0.05 to 1.4 ppqv (Fig. 3), generally lower than previous measurements. It was also lower when compared with the measurements in the Mediterranean as well as Northern Europe (MOE and MAMCS campaigns) (Pirrone et al., 2001, 2003; Sprovieri et al., 2003; Wangberg et al., 2001), but consistent with a few rural sites measurements in the US, such as Chesapeake Bay, Maryland (6–13 pg m^{-3}) (Laurier and Mason, 2007) and Pompano Beach, Florida (1.6–4.9 pg m^{-3}) (Malcom et al., 2003). An apparent characteristic of GOM was its great diversity across US (Fig. 3, Table 3). For coastal sites NH06 and NS01, they showed very low median GOM (0.1 ppqv and 0.05 ppqv) compared with MD08 and MS12 (0.6 ppqv and 0.2 ppqv) even though emission sources within 10 km and 50 km radii of NH06 were no less than those of MS12 and MD08. Variation in wind direction can change the mercury transport pattern; however, GOM is lost quickly from an air mass via dry deposition and its mixing ratio diluted during transport (Valente et al., 2003). The nearby emission sources, if not immediate, may not have significant influences on the GOM levels measured at the monitoring sites.

For inland sites UT97 and UT96, they demonstrated relatively high GOM median levels (1.38 ppqv and 0.49 ppqv, respectively), as well as frequent large spikes in their time series (see Fig. 3). The 2005 NEI facilities emissions data showed that UT96 and UT97 had higher mercury emissions within their 150 km radius (>1.5 T yr^{-1}) compared with other AMNet sites (<0.85 T yr^{-1}), except OH02 (Table 1). Heavy industrial facility emissions could contribute to these characteristics. However, photochemically driven oxidation of GEM is more likely to be responsible for elevated GOM levels in this area. Previous measurements at the Great Salt Lake area reported high mixing ratios of atmospheric reactive chlorine and bromine that could enhance the atmospheric oxidation capacity and thus influence the atmospheric mercury budget in the area (Stutz et al., 2002). At NY95, the median GOM mixing ratio was 0.7 ppqv, the second highest among all the sampling sites. Considering that NY95 has the highest mercury emission sources in its immediate surrounding area (<10 km) (Table 1), this feature probably

ACPD
12, 10845–10878, 2012

resulted from the enhanced local emissions, such as paper production, photographic equipment and nearby coal-fired power plant (from 2005 NEI facilities data). The median GOM mixing ratio at the OH02 site was 0.5 ppqv, only slightly higher than other rural sites; however, the GOM variation (Std. Dev. = 5.2 ppqv) was the largest of all AMNet sites. This implied that the heavy coal combustion emissions had great influence on the GOM fluctuations rather than on the median mixing ratio at OH02 site. In-depth research at OH02 site reported intensive episodic GOM events (GOM > 3.9 ppqv), besides low background concentrations. GOM correlated well with SO_2 (correlation coefficient $r = 0.61$), and even better ($r = 0.80$) during some episodic events (Yatavelli et al., 2006), which supported the hypothesis that local and regional coal-fired power plants may be the primary factor influencing GOM at OH02. The mid-US site in Oklahoma exhibited very low GOM values, probably due to the limited source of direct industrial emissions and lack of halogen oxidants (Table 1).

3.3 PBM

PBM mixing ratios were very different among the AMnet sites (Fig. 3), ranging from 0.18 ppqv to 1.5 ppqv. An interesting and surprising feature of PBM was that its median mixing ratios at all coastal sites were statistically lower ($p \leq 0.001$) than at inland sites, with 0.3 ppqv difference in medians values between coastal and inland sites. The uptake of GEM and GOM by sea salt aerosols was not apparent from the monitoring data, even for the MS12 site which was only 5 km inland from the Gulf of Mexico. This feature may be an artifact due to the inefficiency of the PBM instrument to measure large size aerosols because the elutriator inlet design of the Tekan 1135 removes aerosols >2.5 µm, which could be problematic in the marine environment with sea salt in the 2–10 µm range. Talbot et al. (2011) replaced the elutriator with one that contained no impaction plate to facilitate collection of coarse aerosols on the quartz frit in the Tekran 1135 during a campaign on Appledore Island in the Gulf of Maine and at the coastal site NH06. They found that the Tekan instrument underestimated PBM by as much as a factor of 3 for certain time periods. Thus, it was very likely that PBM in the airshed of

ACPD
12, 10845–10878, 2012

AMNet coastal sites were much higher than the monitoring data suggests. At sites in the Northeast (VT09, NH06, NY20 and NS01) they showed conspicuous seasonality with the highest mixing ratios appearing in winter and spring. High PBM in winter may be caused by colder temperatures and biomass burning in that period (i.e., residential wood burning). Wood smoke with increased potassium and organic carbon concentrations were identified in winter near NY20 sampling site (Choi et al., 2008). Forest fires in springtime can also attribute to elevated PBM mixing ratio. To illustrate this point, Fig. 4 depicts speciated mercury levels in the northeastern US when a forest fire event occurred in Quebec, Canada in late spring 2010. The fire plume was captured by the VT09, NH06, and NY20 sampling sites, inducing elevated speciated mercury levels, especially for PBM. This fire event was also studied by Wang et al. (2010) with focus on mercury mixing ratio and carbonaceous particles around NY20. Besides the obvious enhancement of PBM, high correlation between PBM and Delta-C (Delta-C = Ultraviolet Black Carbon 370 nm absorption – Black Carbon 880 nm absorption), an indicator of wood combustion particles, was found during the fire event.

4 Seasonal trends

On average, GEM was highest in spring at NS01, MS12, NH06, OH02, but peaked in winter at MD08, NY20, VT99 and UT96 (Table 2). For most AMNet sites, the lowest values appeared in fall. High GEM in winter or spring was probably associated with coal and natural gas combustion and increased wood burning for heating during the cold season. In addition, weakened sinks due to the lower atmospheric oxidative capacity and poor vertical mixing caused by a decreased boundary layer height may have led to higher GEM values. Low GEM mixing ratios in warmer seasons were probably due to the increased temperature and solar radiation that favor GEM oxidation. GEM can be transformed to GOM and be subsequently removed from the atmosphere.

Large variations exist in the seasonal median GEM levels in different years and at different sampling sites. The wintertime GEM median mixing ratios in 2007 were higher

ACPD
12, 10845–10878, 2012

than in 2008 (3–56 ppqv higher (Table 2)) and 2009 (5–56 ppqv higher (Table 2)), based on the available data from MS12, MD08, NY20 and VT99. In springtime, the median GEM level at MS12 was about 160 ppqv in all three spring seasons. At MD08 the median values in spring 2008 was 185 ppqv, much higher than at OH02, MS12 and NY20 during the same time period. Springtime GEM at MD08 then decreased to 161 and 164 ppqv in 2009 and 2010, respectively. The wintertime and springtime GEM levels at VT99 were especially higher than at other rural sites, which are probably related to biomass burning (wood burning) in that area. The summer and fall time GEM exhibited large inter-annual differences, which probably were the consequences of different annual meteorological conditions. Monitoring sites, such as MD08, UT97, NY20 and VT99, varried by more than 20 ppqv in summertime median values. MD08, NY20, NH06 and VT99 exhibited large inter-annual differences in the fall seasons.

Higher GOM levels were found in spring at MD08, NH06, NY95, OH02, OK99 and VT99. At other sites, such as NS01, MS12, UT96 and UT97, GOM peaked in summer (Table 3). GOM can be emitted directly from industries, such as coal-fired power plants and waste incinerators, as well as generated from photochemistry reactions of GEM and various oxidants. Higher GOM mixing ratios in spring and summer may be due to the increased length of the growing season at this time, and increasing temperature and radiation (Lai et al., 2012).

PBM is highest in winter at most sites (Table 4). This may result in some locations from wood burning emissions from residential heating. In general, colder temperatures favor partitioning to the aerosol phase (Seinfeld and Pandis, 2006) in addition to decreased removal from the atmosphere (Mao et al., 2011; Amos et al., 2012).

ACPD
12, 10845–10878, 2012

5 Diurnal variation

5.1 GEM

The springtime GEM diurnal variation was modest and averaged 5–16 ppqv in the three spring seasons (Fig. 5, Fig. S1). NY95 and UT97 showed the highest variation amplitudes (11 and 16 ppqv respectively) with similar diurnal patterns that peaked at midnight and dipped around 15:00 local standard time. NY20 exhibited the third highest amplitude variation with the diurnal maxima at 11:00–12:00 eastern standard time (EST), and minima at 05:00 EST.

GEM diurnal variation was most prominent in summer, even though the seasonal median GEM values at most monitoring sites were lower than in spring and winter. The variation amplitudes ranged from 8 ppqv (at MS12) to 55 ppqv (at UT97) in summer 2009 (Fig. 5). Seven rural sites, including MD08, OH02, NH06, NY20, VT99, NS01 and OK99, displayed a similar diurnal pattern in that the lowest GEM levels appeared in the early morning and then increased after sunrise and reached its maxima level at noon or in early afternoon. At MD08, daily minima were found at 05:00 or 06:00 EST, and maxima at 11:00–12:00 EST. OK99 appeared to have a similar diurnal pattern to MD08, and exhibited significantly lower summer GEM levels than in spring (>20 ppqv difference). NY20 showed the lowest mixing ratios at 04:00–05:00 EST in all summer seasons, whose values were even lower than 100 ppqv; highest GEM levels were found at 14:00 EST and the daily difference reached 65 ppqv in 2008, corresponding to about 50 % when referred to the summer average value (Fig. S2). Strong GEM depletion at nighttime was an important feature for the NY20 site. NS01, NH06, VT99 and OH02 also had the daily minimum at 04:00–07:00 local time, and GEM increased until 13:00–14:00 local time. Studies on the CAMNet TGM data found that seven of its rural sites (including the NS01 site) displaced diurnal cycles that had minimum concentrations just before sunrise and maximum concentrations around solar noon, which is similar with our results. The nighttime depletion of TGM underneath the nocturnal inversion layer was considered as the main cause for this pattern (Kellerhals et al., 2003). Mao

ACPD
12, 10845–10878, 2012

et al. (2008) and Talbot et al. (2005) conducted detailed analyses on trace gases at Thompson Farm (NH06), and proposed that the nighttime low levels may result from the presence of the nocturnal inversion layer and chemical and physical processes underneath it. Box model simulations by Kim et al. (2010) further demonstrated that the dissolution of GEM by dew is likely responsible for the low levels of GEM before sunrise. The dissolved GEM then re-volatilizes after sunrise, increasing the GEM mixing ratios in the morning. The maximum GEM mixing ratio at noon or early afternoon was likely due to the morning re-volatilization and downward mixing of remnant boundary layer air (Mao and Talbot, 2011; Selin et al., 2007; Weiss-Penzias et al., 2009). GEM levels decreased when solar radiation reached its maximum, probably a consequence of dilution from increasing boundary layer height and GEM oxidation by photochemical processes to GOM and/or PBM.

Four AMNet sites exhibited different patterns of GEM diurnal variation in summer. The daily dips at MS12 were relatively noticeable at 04:00–06:00 central standard time (CST), whereas the daily peaks were difficult to define. Albeit the fluctuation in 2008 and 2009 were not significant, we observed a weak decrease in GEM around 09:00 CST, much earlier than at the major rural sites. The meteorology in this area may be responsible for this difference; however, the influence of halogen chemistry may also be an important factor for the early decline of GEM. UT96, UT97 and NY95 showed a distinct pattern with the lowest mixing ratios appearing in the afternoon and highest mixing ratios at night. Considering that all these sites are located near lakes, it is possible that the special boundary layer structure and land/lake breeze in those areas caused the unusual variation pattern. Low mercury content air was found at NY95 in summer 2008 when the wind was advected from the northeast over Lake Ontario (Huang et al., 2010). A similar diurnal pattern was found at Reifel Island (CAMNet) site, which was caused by the land breeze advection of urban air to this site at night and lake breeze advection of clean air during daytime (Kellerhals et al., 2003). At UT97, the largest diurnal difference reached 55 ppqv, revealing the exceptionally large daily loss of GEM near the Great Salt Lake.

ACPD
12, 10845–10878, 2012

The fall diurnal variation pattern was similar to that in summer, but with smaller amplitude and lower mixing ratios (Fig. S3). The daily dip at NY20 was dampened, compared with extremely low summertime GEM mixing ratios around mid-night. The winter GEM oscillations were barely noticeable for almost all sites (Fig. S4). It is important to note that the GEM data for this analysis is 3 h resolution data. Mao and Talbot (2011) found larger diurnal variations, ranging from 20 ppqv to 40 ppqv, in summers and falls of 2004–2010 at NH06, by using higher resolution data (i.e., 5 min).

5.2 GOM

Most AMNet sites show a springtime diurnal pattern where the daily maxima appeared at 12:00–16:00 local standard time, and much less noticeable minima around 04:00–06:00 local time (Fig. 6, Fig. S5). The only exception was NY95 in 2010 which showed a different diurnal pattern that dipped at 10:00 and peaked at 18:00 local time. Regarding the difference in variation amplitude, we separated the sampling sites into two groups: (1) the first group included MS12, MD08, OH02, NY95, UT97 and UT96, whose daily oscillation amplitude was >1 ppqv in most spring seasons; and (2) the second group included OK99, NY20, NH06, VT99 and NS01, whose daily variation amplitude was <0.6 ppqv in most spring seasons. The largest GOM daily variation amplitude (2–3 ppqv) was found at UT97, which could be related to the comparatively larger nearby anthropogenic emissions. However, UT97 exhibited large GEM daily variation (16 ppqv), and reduced mixing ratios at daytime while the GOM mixing ratios increased significantly. Thus, photochemical oxidation of GEM was likely a dominant factor controlling GOM.

The summertime daily variation pattern was very similar to that in springtime, whose maxima appeared at 12:00–15:00 and minima appeared at 02:00–05:00 local standard time (Fig. 6). Previous work at NY20 found a daily GOM maximum in the afternoon and minima before sunrise and significantly correlations between GOM and ozone and temperature in summer (Choi et al., 2008). The amplitude variations in summer were generally smaller than in spring, except for 2008 and 2009 at MS12, 2009 of MD08, OK99

ACPD
12, 10845–10878, 2012

and UT97. The first group showed amplitude variation >0.5 ppqv, while the second group was <0.3 ppqv. Utah sites showed significantly larger diurnal variation compared with springtime, probably caused by the increased atmospheric oxidative capacity in summer due to the presence of halogen species. Figure 6 showes that the diurnal variation in 2009 summer at UT96 was more than 2.5 ppqv, while the variation at UT97 site was about 4 ppqv. The largest summer diurnal oscillation was found at UT96 in 2010 summer, demonstrating a 5.2 ppqv variant that was 5-fold of the 2010 summer median level (Fig. S6).

The fall GOM daily variation pattern was very similar to the spring and summer patterns, whose minima appeared after mid-night and maxima appeared in the afternoon (Fig. S7). The diurnal variation amplitudes were also comparable with spring and summertime, although the amplitudes were slightly smaller at a few sites such as VT99 and NS01. The amplitude variation in fall 2009 was smaller than in 2010 at most AMNet sites. In winter, the diurnal variation amplitude dampened, and even became flat at MD08 and OK99 (Fig. S8).

In conclusion, the GOM diurnal fluctuation amplitudes for all seasons at most monitoring sites were in the range of 0 to 2 ppqv, except the especially larger amplitude at the Utah sites. GOM mixing ratios at nighttime were much lower than in daytime. It is interesting to note that the minima in median mixing ratios at MS12 almost reached zero in all spring seasons as well as the summer and fall of 2010, which may be related to the high nighttime air humidity in the Mississippi area that favored the deposition of GOM into dew. Recent research at Thompson Farm, New Hampshire found out that GOM mixing ratios had a decreasing tendency when relative humidity increased, especially in the spring season (Mao et al., 2011).

5.3 PBM

The diurnal variation of PBM can be identified in summer, but it was not apparent in winter despite the highest PBM mixing ratios (Fig. 7). Most sites showed a summertime diurnal pattern with higher values in daytime, and mixing ratios reached their daily

ACPD
12, 10845–10878, 2012

maximum in the early afternoon, and lower mixing ratios appeared at night. This indicates photochemical production or uptake from the gas phase during daytime. However, the Utah sites showed different diurnal patterns with the lowest values appearing in the afternoon, similar to the GEM pattern in that area. UT97 showed lower PBM levels than Antelope Island (UT96), probably due to the elevated altitude of the sampling site. In general, the amplitude of diurnal variation of PBM was much smaller than that of GOM.

6 Summary

Speciated atmospheric mercury data collected at 11 AMNet sites were analyzed in detail for annual, seasonal, and diurnal variations. GEM mixing ratios at these sites were similar and comparable with the current background levels in the Northern Hemisphere. GEM exhibited seasonality with higher mixing ratios appearing in winter and spring and the lowest mixing ratios in fall. A similar diurnal pattern was found in several rural sites, whose lowest levels appeared in the early morning and maxima appeared at noon or in the early afternoon. GEM dissolution in dew at night was considered to be a dominant factor controlling this pattern (Mao and Talbot, 2011).

GOM mixing ratios appeared to be lower than many other GOM measurements around the world, but similar with some rural sites measurements in the US. AMNet data showed a large diversity of GOM values. The higher GOM median mixing ratios appeared in spring and summer, and the largest diurnal variations occurred in spring.

PBM mixing ratios at all coastal AMNet sites were lower than at inland sites. The influence of uptake of GEM and GOM by sea salt aerosols was not apparent, which may due to the deficiency of the PBM instrument to measure large size aerosols. Diurnal variation of PBM can be found in summer instead of winter, albeit the amplitudes were lower than for GOM. High PBM mixing ratios appeared at daytime indicating photochemical production of PBM and uptake from the gas phase.

ACPD
12, 10845–10878, 2012

Supplementary material related to this article is available online at: http://www.atmos-chem-phys-discuss.net/12/10845/2012/acpd-12-10845-2012-supplement.pdf.

Acknowledgements. We thank the AMNet site operators (John Dalziel, Timothy Chang, Dirk Felton, Gary Conley, Larry Scrapper, Neil Olson, Eric Miller, Thomas Holsen) for providing the valuable atmospheric mercury data at all the observational sites. This work was supported by the Environmental Protection Agency under contract #EP09H000355 and the National Oceanographic and Atmospheric Administration under grant #NA07OAR4600514.

References

Amos, H. M., Jacob, D. J., Holmes, C. D., Fisher, J. A., Wang, Q., Yantosca, R. M., Corbitt, E. S., Galarneau, E., Rutter, A. P., Gustin, M. S., Steffen, A., Schauer, J. J., Graydon, J. A., Louis, V. L. St., Talbot, R. W., Edgerton, E. S., Zhang, Y., and Sunderland, E. M.: Gas-particle partitioning of atmospheric Hg(II) and its effect on global mercury deposition, Atmos. Chem. Phys., 12, 591–603, doi:10.5194/acp-12-591-2012, 2012.

Brunke, E. G., Labyschagne, C., and Slemr, F.: Gaseous mercury emissions from a fire in the Cape Peninsula, South Africa, during January 2000, Geophys. Res. Lett., 28, 1483–1496, 2001.

Calvert, J. G. and Lindberg, S. E.: Mechanisms of mercury removal by O_3 and OH in the atmosphere, Atmos. Environ., 18, 3355–3367, 2005.

Choi, H.-D., Holsen, T. M., and Hopke, P. K.: Atmospheric mercury (Hg) in the Adirondacks: Concentrations and sources, Environ. Sci. Technol., 42, 5644–5653, 2008.

Ebinghaus, R., Slemr, F., Brenninkmeijer, C. A. M., van Velthoven, P., Zahn, A., Hermann, M., O'Sullivan, D. A., and Oram, D. E.: Emissions of gaseous mercury from biomass burning in South America in 2005 observed during CARIBIC flights, Geophys. Res. Lett., 34, L08813, doi:10.1029/2006GL028866, 2007.

EPA (United States Environmental Protection Agency): Mercury Study Report to Congress, online available at: www.epa.gov/mercury/report.html, 1997.

ACPD

12, 10845–10878, 2012

Friedli, H. R., Radke, L. F., and Lu, J. Y.: Mercury in smoke from biomass fires, Geophys. Res. Lett., 28, 3223–3226, 2001.
Friedli, H. R., Radke, L. F., Lu, J. Y., Banic, C. M., Leaitch, W. R., and MacPherson, J. I.: Mercury emissions from burning of biomass from temperate North American forests: laboratory and airborne measurements, Atmos. Environ., 37, 253–267, 2003a.
Friedli, H. R., Radke, L. F., Prescott, R., Hobbs, P. V., and Sinha, P.: Mercury emissions from the August 2001 wildfires in Washington State and an agricultural waste fire in Oregon and atmospheric mercury budget estimates, Global Biogeochem. Cy., 17, 1039, doi:10.1029/2002GB001972, 2003b.
Friedli, H. R., Radke, L. F., Prescott, R., Li, P., Woo, J.-H., and Carmichael, G. R.: Mercury in the atmosphere around Japan, Korea, and China as observed during the 2001 ACE-Asia field campaign: Measurements, distributions, sources, and implications, J. Geophys. Res., 109, D19S25, doi:10.1029/2003JD004244, 2004.
Holmes, C. D., Jacob, D. J., and Yang, X.: Global lifetime of elemental mercury against oxidation by atomic bromine in the free troposphere, Geophys. Res. Lett., 33, L20808, doi:10.1029/2006GL027176, 2006.
Holmes, C. D., Jacob, D. J., Corbitt, E. S., Mao, J., Yang, X., Talbot, R., and Slemr, F.: Global atmospheric model for mercury including oxidation by bromine atoms, Atmos. Chem. Phys., 10, 12037–12057, doi:10.5194/acp-10-12037-2010, 2010.
Huang, J., Choi, H.-D., Hopke, P. K., and Holsen, T. M.: Ambient mercury sources in Rochester, NY: results from Principle Components Analysis (PCA) of Mercury Monitoring Network Data, Environ. Sci. Technol., 44, 8441–8445, 2010.
Kellerhals, M., Beauchamp, S., Belzer, W., Blanchard, P.,Froude, F., Harvey, B., McDonald, K., Pilote, M., Poissant, L., Puckett, K., Schroeder, B., Steffen, A., and Tordon, R.: Temporal and spatial variability of total gaseous mercury in Canada: results from the Canadian Atmospheric Mercury Measurement Network (CAMNet), Atmos. Environ., 37, 1003–1011, 2003.
Kim, S. Y.: Continental outflow of polluted air from the U.S. to the North Atlantic and mercury chemical cycling in various atmospheric environments, PhD dissertation, University of New Hampshire, 102, 2010.
Kock, H. H., Bieber, E., Ebinghaus, R., Spain, T. G., and Thees, B.: Comparison of long-term trends and seasonal variations of atmospheric mercury concentrations at the two European coastal monitoring stations Mace Head, Ireland and Zingst, Germany, Atmos. Environ., 39, 7549–7556, 2005.

ACPD
12, 10845–10878, 2012

Lai, Z. L., Talbot, R., and Mao, H.: Recant decadal ozone trends at rural sites in New England, USA, Atmos. Chem. Phys., submitted, 2012.
Laurier, F. J. G., Mason, R. P., and Whalin, L.: Reactive gaseous mercury formation in the North Pacific Ocean's marine boundary layer: A potential role of halogen chemistry, J. Geophys. Res., 108, 4529, doi:10.1029/2003JD003625, 2003.
Laurier, F. and Mason, R.: Mercury concentration and speciation in the coastal and open ocean boundary layer, J. Geophys. Res. D, 112, D06302, doi:10.1029/2006JD007320, 2007.
Lindberg, S. E. and Stratton, W. J.: Atmospheric mercury speciation: concentrations and behavior of reactive gaseous mercury in ambient air, Environ. Sci. Technol., 32, 49–57,1998.
Malcolm, E. G., Keeler, G. J., and Landis, M. S.: The effects of the coastal environment on the atmospheric mercury cycle, J. Geophys. Res., 108, 4357, doi:10.1029/2002JD003084, 2003.
Mao, H., Talbot, R. W., Sigler, J. M., Sive, B. C., and Hegarty, J. D.: Seasonal and diurnal variations of Hg^0 over New England, Atmos. Chem. Phys., 8, 1403–1421, doi:10.5194/acp-8-1403-2008, 2008.
Mao, H. and Talbot, R.: Speciated mercury at marine, coastal, and inland sites in New England – Part 1: Temporal variability, Atmos. Chem. Phys. Discuss., 11, 32301–32336, doi:10.5194/acpd-11-32301-2011, 2011.
Mao, H., Talbot, R., Hegarty, J., and Koermer, J.: Speciated mercury at marine, coastal, and inland sites in New England – Part 2: Relationships with atmospheric physical parameters, Atmos. Chem. Phys. Discuss., 11, 28395–28443, doi:10.5194/acpd-11-28395-2011, 2011.
Pacyna, E. G. and Pacyna, J. M.: Global emission of mercury from anthropogenic sources in 1995, Water Air Soil Pollut., 137, 149–165, 2002.
Pacyna, E. G., Pacyna, J. M., Steenhuisen, F., and Wilson, S.: Global anthropogenic mercury emission inventory for 2000, Atmos. Environ., 40, 4048–4063, 2006.
Pacyna, E. G., Pacyna, J. M., Sundseth, K., Munthe, J., Kindbom, K., Wilson, S., Steenhuisen, F., and Maxson, P.: Global emission of mercury to the atmosphere from anthropogenic sources in 2005 and projections to 2020, Atmos. Environ., 44, 2487–2499, 2010.
Pal, B. and Ariya, P. A.: Studies of ozone initiated reactions of gaseous mercury: kinetics, product studies, and atmospheric implications, Phy. Chem. Chem. Phy., 6, 572–579, 2004a.
Pal, B. and Ariya, P. A.: Gas-phase HO^0-initiated reactions of elemental mercury: kinetics, product studies, and atmospheric implications, Environ. Sci. Technol., 38, 5555–5566, 2004b.

ACPD
12, 10845–10878, 2012

Peterson, C., Gustin, M., and Lyman, S.: Atmospheric mercury concentrations and speciation measured from 2004 to 2007 in Reno, Nevada, USA, Atmos. Environ., 43, 4646–4654, 2009.
Pirrone, N., Costa,P., Pacyna, J. M., and Ferrara, R.: Mercury emissions to the atmosphere from natural and anthropogenic sources in the Mediterranean region, Atmos. Environ., 35, 2997–3006, 2001.
Raofie, F. and Ariya, P. A.: Product study of the gas-phase BrO-initiated oxidation of Hg0: evidence for stable Hg1 compounds, Environ. Sci. Technol., 38, 4319–4326, 2004.
Selin, N. E., Jacob, D. J., Park, R. J., Yantosca, R. M., Strode, S., Jaegle' L., and Jaffe D.: Chemical cycling and deposition of atmospheric mercury: Global constraints from observations, J. Geophys. Res., 112, D02308, doi:10.1029/2006JD007450, 2007.
Seigneur, C., Vijayaraghavan, K., Lohman, K., Karamchandani, P., and Scott, C.: Global source attribution for mercury deposition in the United States, Environ. Sci. Technol., 38, 555–569, 2004.
Seigneur, C., Vijayaraghavan, K., and Lohman, K.,: Atmospheric mercury chemistry: Sensitivity of global model simulations to chemical reactions, J. Geophys. Res., 111, D22306, doi:10.1029/2005JD006780, 2006.
Seinfeld, J. H. and Pandis, S. N.: Atmospheric Chemistry and Physics: from Air Pollution to Climate Change, John Wiley, New York, 2006.
Sigler, J. M., Lee, X., and Munger, W.: Emission and long-range transport of gaseous mercury from a large-scale Canadian boreal forest fire, Environ. Sci. Technol., 37, 4343–4347, 2003.
Sigler, J. M. and Lee, X.: Gaseous mercury in background forest soil in the northeastern United States, J. Geophys. Res., 111, G02007, doi:10.1029/2005JG000106, 2006.
Sigler, J. M., Mao, H., Sive, B. C., and Talbot, R.: Oceanic influence on atmospheric mercury at coastal and inland sites: a springtime noreaster in New England, Atmos. Chem. Phys., 9, 4023–4030, doi:10.5194/acp-9-4023-2009, 2009.
Sommar, J., Hallquist, M., Ljungström, E., and Lindqvist, O.: On the gas phase reactions between volatile biogenic mercury species and the nitrate radical, J. Atmos. Chem., 27, 233–247, 1997.
Sommar, J., Gardfeldt, K., Stromberg, D., and Feng, X.: A kinetic study of the gas-phase reaction between the hydroxyl radical and atomic mercury, Atmos. Environ., 35, 3049–3054, 2001.

ACPD
12, 10845–10878, 2012

Sprovieri, F., Pirrone, N., Gardfeldt., K., and Sommar, J.: Mercury speciation in the marine boundary layer along a 6000 km cruise path around the Mediterranean Sea, Atmos. Environ., 37, S6371, 21–39, 2003.

Sprovieri, F., Pirrone, N., Ebinghaus, R., Kock, H., and Dommergue, A.: A review of worldwide atmospheric mercury measurements, Atmos. Chem. Phys., 10, 8245–8265, doi:10.5194/acp-10-8245-2010, 2010.

Stutz, J., Ackermann, R., Fast, J. D., and Barrie, L.: Atmospheric reactive chlorine and bromine at the Great Salt Lake, Utah, Geophys. Res. Lett., 29, 1380, doi:10.1029/2002GL014812, 2002.

Talbot, R., Mao, H., and Sive, B.: Diurnal characteristics of surface-level O_3 and other important trace gases in New England, J. Geophys. Res., 110, D09307, doi:10.1029/2004JD005449, 2005.

Talbot, R., Mao, H., Feddersen D., Smith, M., Kim, S. Y., Sive, B., Haase, K., Ambrose, J., Zhou, Y., and Russo, R.: Comparison of particulate mercury measured with manual and automated methods, Atmosphere, 2, 1–20, doi:10.3390/atmos2010001, 2011.

Temme, C., Blanchard, P., Steffen, A., Banic, C., Beauchamp, S., Poissant, L., Tordon, R., and Wiens, B.: Trend, seasonal and multivariate analysis study of total gaseous mercury data from the Canadian atmospheric mercury measurement network (CAMNet), Atmos. Environ., 41, 5423–5441, doi:10.1016/j.atmosenv.2007.02.021, 2007.

Valente, R. J., Shea, C., Humes, K. L., and Tanner, R. L.: Atmospheric mercury in the Great Smoky Mountains compared to regional and global levels, Atmos. Environ., 41, 1861–1873, 2007.

Wangberg, I., Munthe, J., Pirrone, N., Iverfeldt, A., Bahlman, E.,Costa, P., Ebinghaus, R., Feng, X., Ferrara, R., Gardfeldt, K., Kock, H., Lanzillotta, E., Mamane, Y., Mas, F., Melamed, E., Osnat, Y., Prestbo, E., Sommar, J., Schmolke, S., Spain, G., Sprovieri, F., and Tuncel, G.: Atmospheric mercury distribution in Northern Europe and in the Mediterranean region, Atmos. Environ., 35, 3019–3025, 2001.

Wang, Y., Huang, J., Zananski, T. J., Hopke, P. K., and Holsen, T. M.: Impacts of the Canadian Forest Fires on Atmospheric Mercury and Carbonaceous Particles in Northern New York, Environ. Sci. Technol., 44, 8435–8440, 2010.

Weiss-Penzias, P., Gustin, M. S., and Lyman, S. N.: Observations of speciated atmospheric mercury at three sites in Nevada: Evidence for a free tropospheric source of reactive gaseous mercury, J. Geophys. Res., 114, D14302, doi:10.1029/2008JD011607, 2009.

ACPD
12, 10845–10878, 2012

Weiss-Penzias, P., Jaffe, D. A., McClintick, A., Prestbo, E. M., and Landis, M. S.: Gaseous elemental mercury in the marine boundary layer: evidence for rapid removal in anthropogenic pollution, Environ. Sci. Technol., 37, 3755–3763, 2003.

Yatavelli, R. L. N., Fahrni, J. K., Kim, M., Crist, K. C., Vickers, C. D., Winter, S. E., and Connell, D. P.: Mercury, $PM_{2.5}$ and gaseous co-pollutants in the Ohio River Valley region: Preliminary results from the Athens supersite, Atmos. Environ., 40, 6650–6665, doi:10.1016/j.atmosenv.2006.05.072, 2006.

ACPD

12, 10845–10878, 2012

Table 1. Site description and mercury emission from nearby facilities.

Site ID	Site Name	Latitude	Longitude	Elevation	Type	Emission sources at <10 km ($T\,yr^{-1}$)*	Emission sources at 10–50 km ($T\,yr^{-1}$)*	Emission sources at 50–150 km ($T\,yr^{-1}$)*
MS12	Grand Bay NERR	30.4294	−88.4277	2	Rural	0	0.081	0.214
MD08	Piney Reservoir	39.7053	−79.0122	769	Rural	1.003×10^{-5}	0.015	0.729
OK99	Stilwell	35.7514	−94.6717	304	Rural	2.941×10^{-10}	0.001	0.841
UT96	Antelope Island	41.0467	−112.0248		Rural	4.513×10^{-9}	0.082	1.489
UT97	Salt Lake City	40.7118	−111.9609	1297	Urban	1.034×10^{-4}	0.134	1.432
OH02	Athens Super Site	39.3078	−82.1182	275	Rural	1.485×10^{-3}	0.001	9.168
NY20	Huntington Wildlife	43.9731	−74.2231	500	Rural	0	1.702×10^{-5}	0.562
NY95	Rochester	43.1463	−77.5481	136	Suburban	0.079	0.046	0.327
NH06	Thompson Farm	43.1100	−70.9500		Rural	1.266×10^{-3}	0.064	0.259
VT99	Underhill	41.0467	−112.0248	399	Rural	0	0.006	0.100
NS01	Kejimkujik National Park	44.4328	−65.2056	155	Rural	NA	NA	NA

* Calculated from US EPA's 2005 National Emission Inventory point sources (facilities) data (http://www.epa.gov/ttn/chief/net/2005inventory.html).

ACPD
12, 10845–10878, 2012

Table 2. The seasonal and total medians of GEM at 11 AMNet sites.

	MS12	MD08	OK99	UT96	UT97	OH02	NY20	NY95	NH06	VT99	NS01
Winter 07	163	192					219			197	
Winter 08	160	162			212	153	163	169	150	183	
Winter 09	158	169	169	184	233	160	163	158		177	158
Winter Ave	161	174	169	184	223	157	182	163	150	186	158
Spring 08	161	185				160	151			190	
Spring 09	163	161	157		224	155	160	165	169	175	169
Spring 10	160	164	170	177	225	177	153	161	150	182	
Spring Ave	161	170	164	177	225	164	155	163	160	182	169
Summer 08	145	155				159	144			160	
Summer 09	158	127	138	176	237	144	122	149	141	138	142
Summer 10		147	144	174	214	154	139	152	151	162	
Summer Ave	151	143	141	175	226	152	135	151	146	153	142
Fall 08	147	142				157	144	157		148	
Fall 09	143	127	141	166	221	142	119	138	119	136	131
Fall 10	153	147	142	180		147	135		142	164	
Fall Ave	148	139	142	173	221	149	132	147	130	149	131
Total Median	157 ± 25	156 ± 28	153 ± 25	176 ± 95	226 ± 95	155 ± 173	148 ± 49	158 ± 36	149 ± 23	167 ± 27	156 ± 34

Total Median: median ± standard deviation.

ACPD
12, 10845–10878, 2012

Table 3. The seasonal and total medians of GOM at 11 AMNet sites.

	MS12	MD08	OK99	UT96	UT97	OH02	NY20	NY95	NH06	VT99	NS01
Winter 07	0.17	1.54					0.27			0.29	
Winter 08	0.11	0.44			0.83	0.34	0.08	0.28	0.09	0.12	
Winter 09	0.19	0.61	0.07	0.16	3.06	0.52	0.09	1.64		0.26	0.02
Winter Ave	0.16	0.86	0.07	0.16	1.94	0.43	0.15	0.96	0.09	0.23	0.02
Spring 08	0.25	1.89				0.98	0.17			0.43	
Spring 09	0.18	0.81	0.21		0.89	0.88	0.08	0.50	0.41	0.25	0.12
Spring 10	0.27	0.55	0.10	0.36	1.23	0.80	0.10	2.89	0.13	0.61	
Spring Ave	0.23	1.08	0.16	0.36	1.06	0.89	0.12	1.69	0.27	0.43	0.12
Summer 08	0.33	1.16				0.44				0.05	
Summer 09	0.36	0.64	0.10	1.47	1.81	0.20		0.38	0.10		0.26
Summer 10		0.36	0.06	1.05	2.49	0.17	0.10	0.34	0.05	0.09	
Summer Ave	0.35	0.72	0.08	1.26	2.15	0.27	0.10	0.36	0.08	0.07	0.26
Fall 08	0.19	0.34				0.66		0.82		0.04	
Fall 09	0.30	0.53	0.07	0.56	1.22	0.57		1.39	0.11		0.02
Fall 10	0.24	0.47	0.10	0.96		0.50	0.28		0.05	0.04	
Fall Ave	0.24	0.44	0.08	0.76	1.22	0.58	0.28	1.11	0.08	0.04	0.02
Total Median	0.22 ± 1.58	0.63 ± 1.70	0.10 ± 0.49	0.49 ± 2.58	1.38 ± 3.80	0.47 ± 5.17	0.06 ± 0.33	0.74 ± 1.58	0.10 ± 0.45	0.13 ± 0.73	0.05 ± 0.45

Total Median: median ± standard deviation.

ACPD
12, 10845–10878, 2012

Table 4. The seasonal and total medians of PBM at 11 AMNet sites.

	MS12	MD08	OK99	UT96	UT97	OH02	NY20	NY95	NH06	VT99	NS01
Winter 07	0.32	1.05					2.00			2.42	
Winter 08	0.34	0.33			1.62	0.81	0.42	1.56	0.09	1.77	
Winter 09	0.67	0.49	0.39	1.71	0.81	1.44	0.35	1.68		1.34	0.18
Winter Ave	0.44	0.62	0.39	1.71	1.22	1.13	0.92	1.62	0.09	1.84	0.18
Spring 08	0.28	0.87				0.86	0.80			1.52	
Spring 09	0.24	0.13	0.45		0.56	0.84	0.14	1.00	0.27	1.01	0.53
Spring 10	1.18	0.43	0.36	0.71	0.19	0.72	0.46	2.30	0.19	0.65	
Spring Ave	0.56	0.48	0.40	0.71	0.37	0.81	0.47	1.65	0.23	1.06	0.53
Summer 08	0.25	0.65				0.45	0.09			0.43	
Summer 09	0.16	0.21	0.43	1.43	0.84	0.32	0.14	0.65	0.22	0.31	0.16
Summer 10		0.38	0.34	1.13	0.12	0.45	0.46	2.23	0.33	0.21	
Summer Ave	0.20	0.42	0.39	1.28	0.48	0.41	0.23	1.44	0.27	0.32	0.16
Fall 08	0.51	0.11				0.45		1.31		0.38	
Fall 09	0.31	0.29	0.28	1.15	0.82	0.49	0.08	1.29	0.04	0.38	
Fall 10	0.32	0.38	0.35	1.14		0.66	0.42		0.10	0.09	
Fall Ave	0.38	0.26	0.31	1.15	0.82	0.53	0.25	1.30	0.07	0.29	0.09
Total Median	0.32 ± 1.29	0.31 ± 0.58	0.37 ± 0.36	1.16 ± 4.11	0.66 ± 6.98	0.60 ± 6.47	0.24 ± 0.76	1.53 ± 1.26	0.18 ± 0.36	0.56 ± 1.60	0.27 ± 0.66

Total Median: median ± standard deviation.

ACPD
12, 10845–10878, 2012

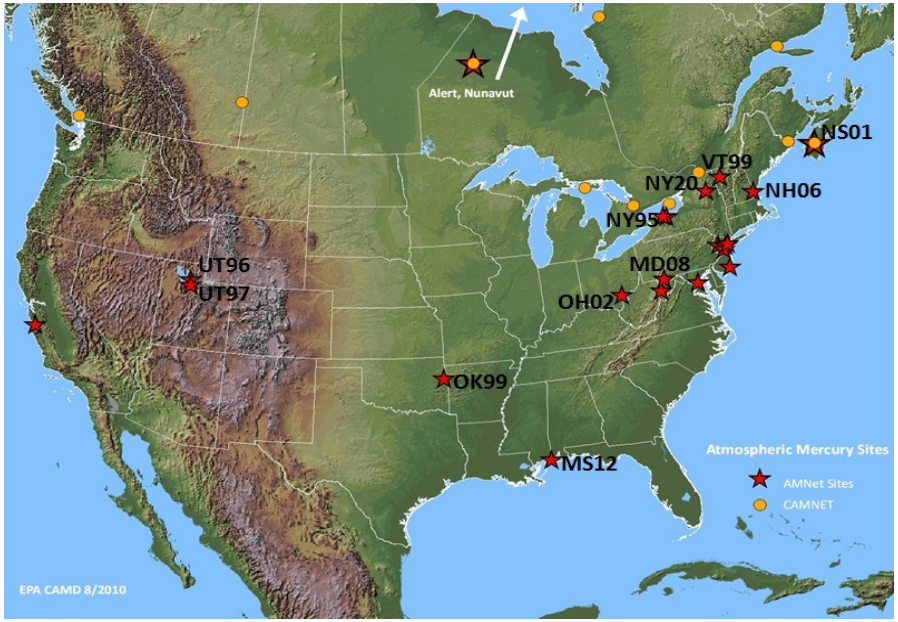

Fig. 1. Locations of 11 AMNet sites utilized in this study.

ACPD
12, 10845–10878, 2012

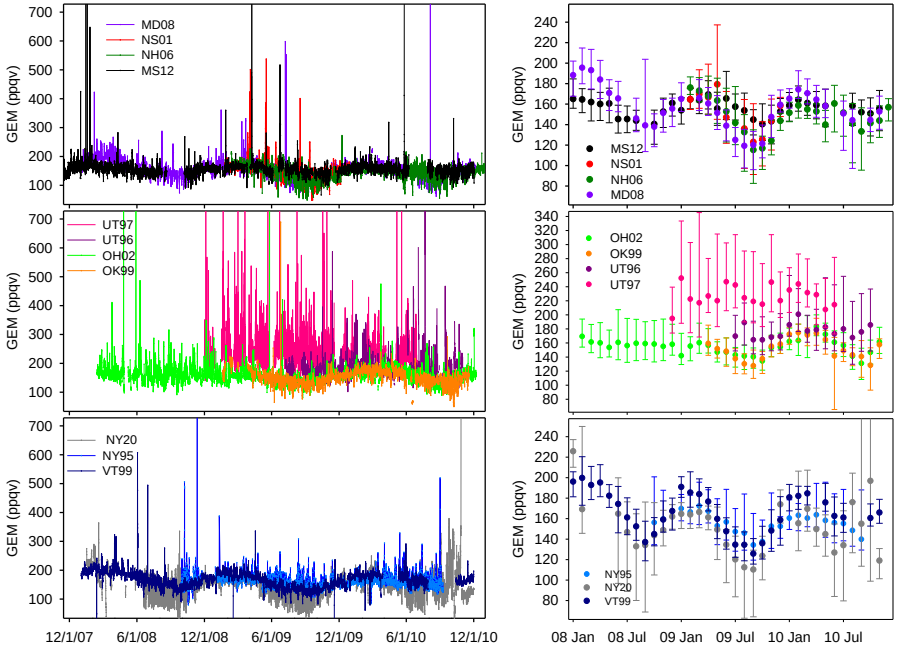

Fig. 2. Complete time series of GEM (left panel) and the monthly median mixing ratio at 11 sites, the upper error bars represent 90 percentile while the lower error bars represent 10 percentile values (right panel).

ACPD
12, 10845–10878, 2012

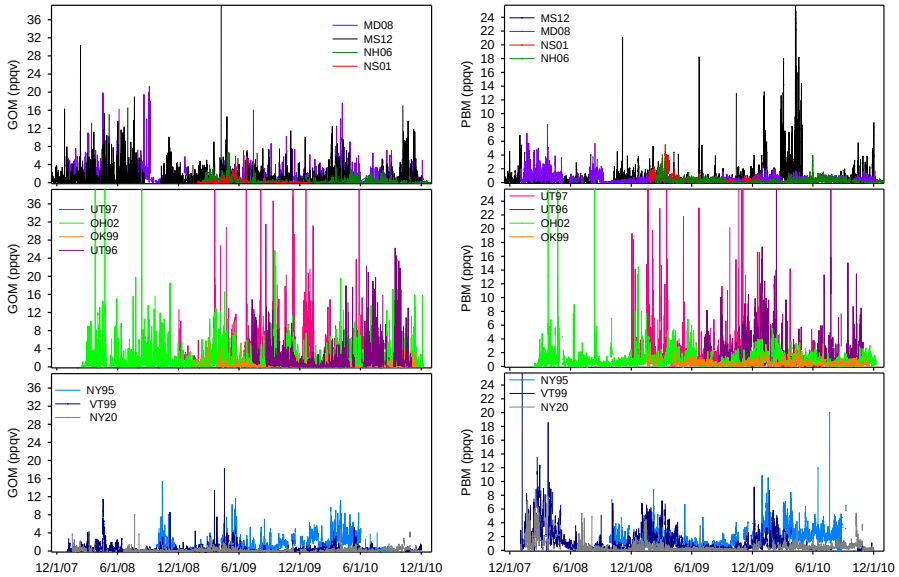

Fig. 3. Complete time series of GOM (left panel) and PBM (right panel).

ACPD
12, 10845–10878, 2012

Seasonal and diurnal variations of atmospheric mercury

X. Lan et al.

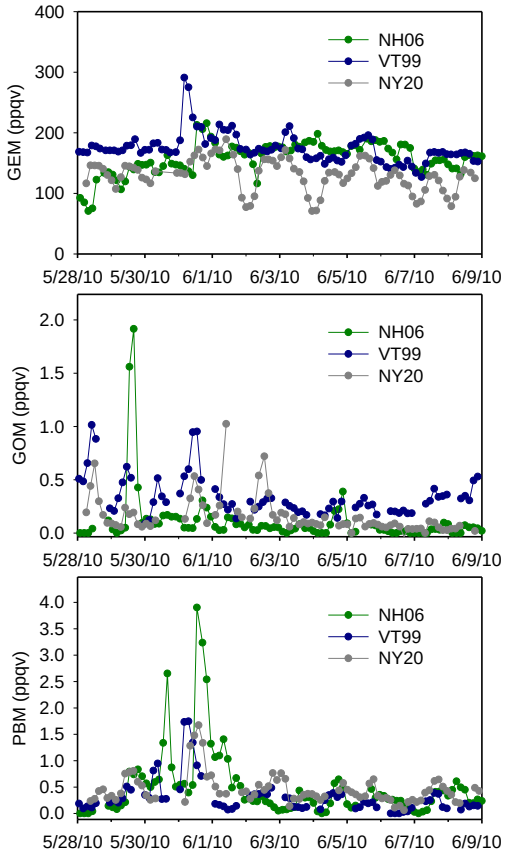

Fig. 4. Speciated mercury mixing ratio during the 2010 spring Quebec fire event.

ACPD
12, 10845–10878, 2012

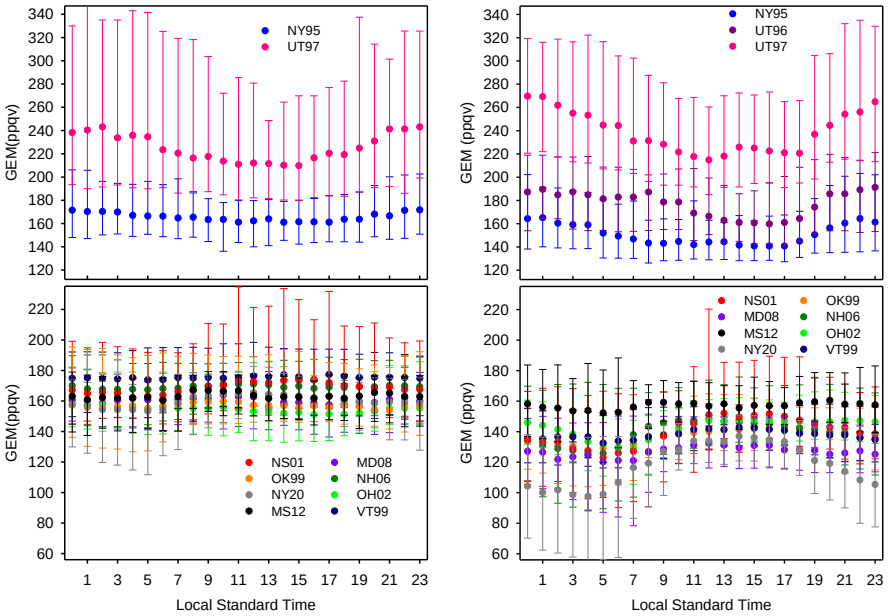

Fig. 5. GEM diurnal variation in 2009 spring (left panel) and 2009 summer (right panel), the upper error bars represent 90 percentile while the lower error bars represent 10 percentile values.

ACPD
12, 10845–10878, 2012

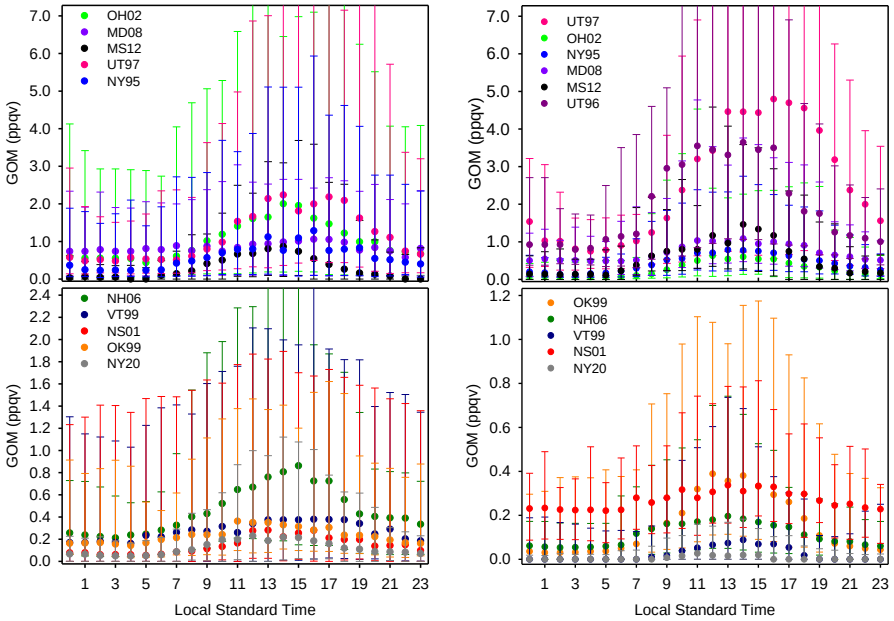

Fig. 6. GOM diurnal variation in 2009 spring (left panel) and 2009 summer (right panel), the upper error bars represent 90 percentile while the lower error bars represent 10 percentile values.

ACPD
12, 10845–10878, 2012

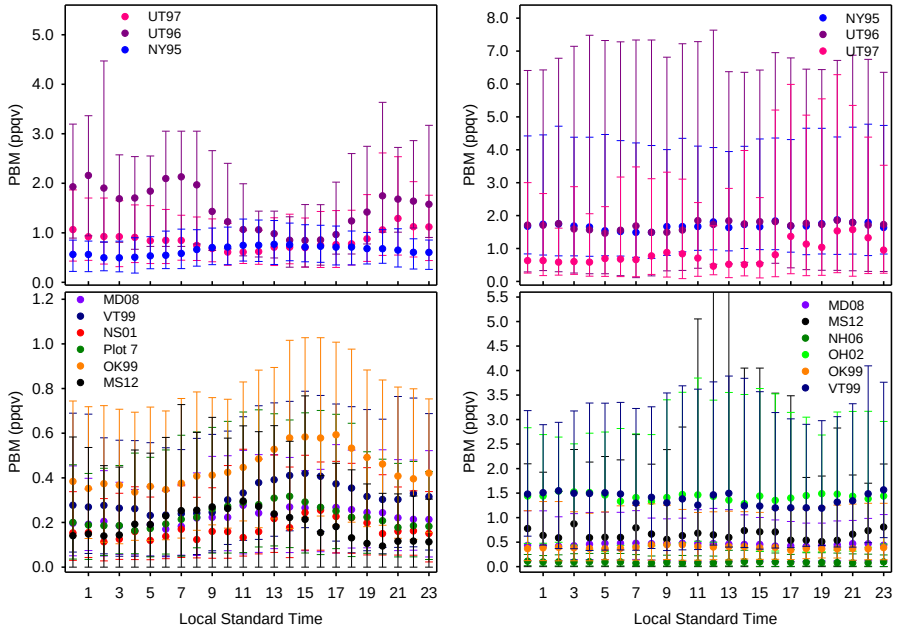

Fig. 7. PBM diurnal variation in 2009 summer (left panel) and winter (right panel), the upper error bars represent 90 percentile while the lower error bars represent 10 percentile values.

ACPD
12, 10845–10878, 2012

Seasonal and diurnal variations of atmospheric mercury

X. Lan et al.